A Cellular Potts Model of the interplay of synchronization and aggregation

Rose Una and Tilmann Glimm

Department of Mathematics, Western Washington University, Bellingham, WA, United States of America

ABSTRACT

We investigate the behavior of systems of cells with intracellular molecular oscillators ("clocks") where cell-cell adhesion is mediated by differences in clock phase between neighbors. This is motivated by phenomena in developmental biology and in aggregative multicellularity of unicellular organisms. In such systems, aggregation co-occurs with clock synchronization. To account for the effects of spatially extended cells, we use the Cellular Potts Model (CPM), a lattice agent-based model. We find four distinct possible phases: global synchronization, local synchronization, incoherence, and anti-synchronization (checkerboard patterns). We characterize these phases via order parameters. In the case of global synchrony, the speed of synchronization depends on the adhesive effects of the clocks. Synchronization happens fastest when cells in opposite phases adhere the strongest ("opposites attract"). When cells of the same clock phase adhere the strongest ("like attracts like"), synchronization is slower. Surprisingly, the slowest synchronization happens in the diffusive mixing case, where cell-cell adhesion is independent of clock phase. We briefly discuss potential applications of the model, such as pattern formation in the auditory sensory epithelium.

Subjects Biophysics, Computational Biology, Evolutionary Studies, Mathematical Biology

Keywords Cellular Potts Model, Synchronization, Aggregation, Biological clocks, Mathematical modeling

Submitted 6 September 2023
Accepted 29 January 2024
Published 29 February 2024

Corresponding author
Tilmann Glimm, glimmt@wwu.edu

Academic editor
Joseph Gillespie

Additional Information and Declarations can be found on page 15

DOI **10.7717/peerj.16974**

INTRODUCTION

Synchronization of coupled oscillators is a common phenomenon in nature, for instance the emergence of synchrony in neural networks (*Singer, 1999*; *Hansel, Mato & Meunier, 1995*; *Uhlhaas et al., 2009*), the synchronization of fireflies flashing (f.ex. *Faust, 2010*; *Ramírez-Ávila et al., 2019*; *Sokol, 2022*), the coordination of circadian rhythms in eusocial colonies (*Siehler, Wang & Bloch, 2021*; *Frisch & Koeniger, 1994*) or the synchronization of intracellular molecular oscillatory processes in developmental biology (*Jiang et al., 2000*; *Bhat et al., 2019*; *Venzin & Oates, 2020*; *Deneke et al., 2016*). Beginning with the seminal works of Winfree (*e.g.*, *Winfree, 1987*) and Kuramoto (*e.g.*, *Kuramoto, 1984*) in the 1970s, mathematical models of synchronization phenomena in networks of coupled oscillators have been an intense area of study; see *e.g.*, the books by *Pikovsky, Rosenblum & Kurths (2003)* and *Boccaletti et al. (2018)*, or surveys by *Dörfler & Bullo (2014)* and *Rodrigues et al. (2016)*.

The interplay of synchronization and spatial aggregation in systems of *moving* interacting oscillators is much less well studied in models. The most influential work in this direction is the investigation of swarming oscillators ("swarmalators") by *OKeeffe, Hong & Strogatz*

(2017) and subsequent works by Sar et al. (2022), OKeeffe, Ceron & Petersen (2022) and Barciś & Bettstetter (2020). These "swarmalators" are mass points with internal oscillators ("clocks") which attract or repel each other according to their clock phase difference, and also interact with each other *via* Kuramoto-like interactions.

One important potential application of systems of interacting moving oscillators is the aggregation of biological cells mediated by cell–cell adhesion in aggregative multicellularity, *e.g.*, the slime bacteria myxobacteria (Shimkets & Kaiser, 1982; Zusman et al., 2007; Peruani et al., 2012; Thutupalli et al., 2015), or the slime mold *Dictyostelium discoideum* (Bonner, 2008; Van Oss et al., 1996; Marée & Hogeweg, 2001). Indeed, these two systems also exhibit intracellular oscillators (Gregor et al., 2010; Alber, Jiang & Kiskowski, 2004; Guzzo et al., 2018; Arias Del Angel et al., 2020).

Another application is in vertebrate embryogenesis, where members of the Hes gene family, which is known to play a central roles in determining cell fate in development, display sustained intracellular oscillations in expression patterns (Kageyama, Ohtsuka & Kobayashi, 2007; Hirata et al., 2002). Synchronized Hes oscillations are crucial for somitogenesis (recently reviewed by Carraco, Martins-Jesus & Andrade (2022)), providing the experimental foundation for the famed clock and wavefront model of somite pattern formation originally proposed by Cooke & Zeeman (1976), see also Murray, Maini & Baker (2011). Another example of the interplay of spatial pattern formation and intracellular oscillators is in vertebrate limb development, where Hes1 was found to play a role in regularizing the spatial pattern of precartilage condensations, aggregates of mesenchymal cells (Bhat et al., 2019; Newman, Bhat & Glimm, 2021). While there is no known direct link between the Hes family and cell–cell adhesion, there is a well-established link between Notch signaling and Hes expression Kageyama, Shimojo & Isomura (2018), Kageyama, Ohtsuka & Kobayashi (2007). The Notch pathway controls cell communication between neighboring cells, but also may directly mediate cell–cell adhesion (Murata & Hayashi, 2016), making assumed mutual interdependence between intracellular oscillations and cell–cell adhesion plausible.

Motivated by this, Glimm & Gruszka (2024) recently suggested a partial differential equations (PDE) model that takes into account local cell–cell adhesion (as opposed to attraction independent of the distance of two cells as in O'Keefe et al.'s swarmalators), as well as a local Kuramoto-like interaction of oscillators. In a linear stability analysis, they identfied a number of emerging behaviors –the possibility of aggregation or dispersion can be combined with either global synchronization, only local synchronization (synchronized patches), or incoherence.

A PDE model has the advantage of being amenable to analytic methods, but has the drawback of dealing with cell *densities* instead of modeling cells individually. This means that the effects of variations of cell size and shape are not modeled. To address this, we present a model based in part on the work of OKeeffe, Hong & Strogatz (2017) and Glimm & Gruszka (2024), but where cells are modeled *via* the Cellular Potts Model (CPM) (Graner & Glazier, 1992). The CPM, also known as the Glazier-Graner-Hogeweg model, is a computational lattice-based model that allows for spatially extended cells and incorporates fluctuations in cell size and cell shape.

Our minimalistic model incorporates cells with an intracellular oscillator. We subsume the complex dynamics of intracellular oscillations into a single variable and assume that adhesion between two cells depends on the relative oscillator phases, and that adjacent cells influence each others' oscillators. (Portions of this text were previously published as part of a thesis; see *Una, 2023*). More specifically, in our CPM framework, each cell is associated with an internal oscillator, or cell clock. Clocks interact locally *via* Kuramoto-like interactions, where the type and strength of interactions is encapsulated by a parameter K. Cell–cell adhesion between neighboring cells is influenced by the clock phase differences with three different qualitative possibilites encoded by a parameter J: "like attracts like", where cells in the same phase adhere to each other maximally ($J > 0$); "opposites attract", where cells in opposite phases adhere to each other maximally ($J < 0$); and the purely diffusive case where cell–cell adhesion is independent of clocks ($J = 0$). We investigate the effects of the parameters J and K on oscillator synchronization and spatial aggregation. We find four distinct types of steady phase states emerging from random initial conditions: global synchronization, local synchronization, incoherence, and anti-synchronization (checkerboard pattern). We define the four distinct phase states qualitatively with a phase diagram and quantitatively with order parameters. Of particular interest is the case of global synchronization, which occurs when the Kuramoto interaction parameter K is positive, *i.e.,* neighboring cells seek to synchronize their clocks. Here we find that initially, synchronization advances fastest for negative J and slowest for positive J. But in the long run, remarkably, synchronization is slowest in the "border case" $J = 0$, *i.e.,* the purely diffusive case when cell–cell adhesion is independent of clock phase. We give an intuitive explanation of this phenomenon.

Our work is a high-level generic model of the interplay of intracellular oscillations and cell–cell adhesion. It is motivated by examples from development biology and aggregative multicellularity, but is not a model of a specific experiment. Instead, we seek to provide an investigation of the broad types of patterns in space and synchronizations that are possible with a set of minimal assumptions. However, we discuss potential applications to concrete findings about pattern formation in the auditory sensory epithelia of many species, where checkerboard patterns composed of sensory hair and supporting cells are established in development and crucial for proper functioning (*Togashi et al., 2011*; *Katsunuma et al., 2022*).

METHODS

The model

The model uses the framework of the Cellular Potts Model (CPM; see *Graner & Glazier (1992)*) based on a rectangular lattice. Each cell is modeled as a group of lattice sites and is associated with an internal oscillator ("clock"). Adhesion between cells is incorporated into the model *via* the Hamiltonian, an energy function. Time evolution is modeled *via* an energy minimization procedure in space and an updating rule for the clocks. (See Fig. 1 for a sketch of the schematics of the CPM.)

More specifically, lattice sites are denoted by bold variables $\mathbf{i} = (i_1, i_2)$ or $\mathbf{j} = (j_1, j_2)$. At every time step, each lattice site $\mathbf{i}$ belongs to one of N cells or to the extracellular matrix

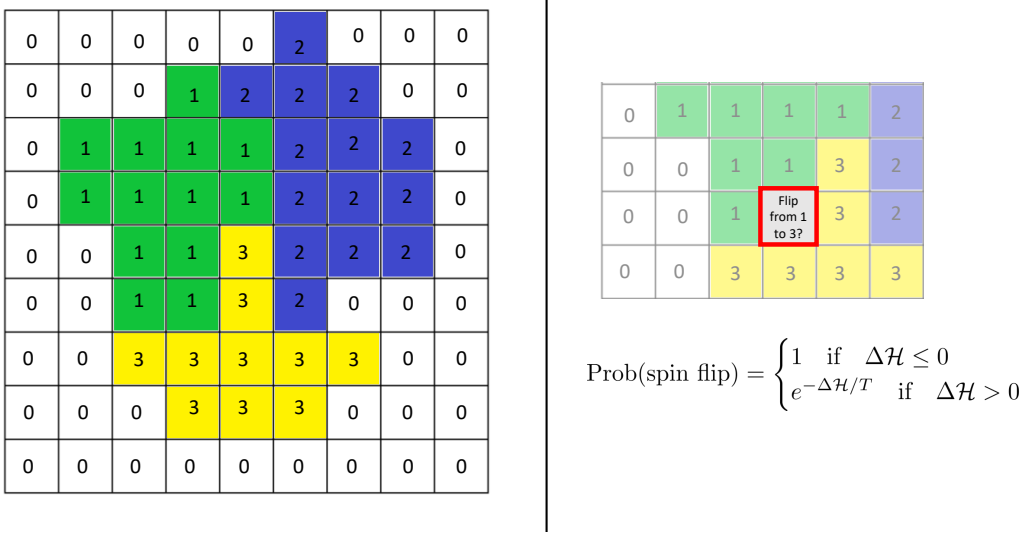

Figure 1 **Schematics of the cellular potts model.** Left: Cells are modeled as sets of lattice sites. We picture three cells with indices ("spins") 1–3. The index 0 denotes the extracellulcar matrix (medium). Each cell has a clock whose current value is represented by the color of the cell. Each configuration of the lattice has a Hamiltonian (energy) $\mathcal{H}$, which encodes various biological phenomena such as adhesion and elasticity. Right: Time evolution is modeled *via* so-called "spin flips". A lattice site is chosen at random and a change of its index to that of a neighboring cell is proposed. This change is accepted with the displayed probability which depends on the change $\Delta\mathcal{H}$ in the Hamiltonian it causes. Here T is a given constant, the "temperature." See the text for more details.

Full-size DOI: 10.7717/peerj.16974/fig-1

(ECM). Cells are numbered with an index that ranges from 1 to N. We use the notation $\sigma^t(\mathbf{i}) = 0$ if the site $\mathbf{i}$ belongs to the medium at time step t, and $\sigma^t(\mathbf{i}) = s$ if $\mathbf{i}$ belongs to the sth cell ($s = 1, \ldots, N$). Additionally, each cell $s = 1, \ldots, N$ has an internal clock. This clock is a time-dependent scalar θ_s^t. For notational simplicity, we will suppress the superscript t unless necessary.

The governing Hamiltonian is

$$\mathcal{H} = \sum_{\substack{\text{neighboring} \\ \text{lattice sites } \mathbf{i},\mathbf{j}}} (1 - \delta_{\sigma(\mathbf{i}),\sigma(\mathbf{j})}) f(\sigma(\mathbf{i}), \sigma(\mathbf{j})) + \lambda \sum_{\text{cell } s} (\text{Area}(s) - A_{\text{target}})^2. \tag{1}$$

The Hamiltonian encodes the compressibility of the cells and cell–cell adhesion. The second term of the Hamiltonian is a cell area constraint term. Here $A(s)$ is the area of the cell with index s, *i.e.,* the number of lattice sites it occupies. A_{target} is the target area, a fixed reference area, and λ is a parameter that encodes the compressibility of the cell: the larger λ is, the less fluctuations in size there are. (Our choices of A_{target} and λ are based on the work of *Zhang et al. (2011)*; see Table 1.)

Crucially, the first term of the Hamiltonian describes cell–cell adhesion between adjacent cells. The symbol δ_{ij} is the Kronecker delta: $\delta_{i,j} = 1$ if $i = j$, and $\delta_{i,j} = 0$ if $i \neq j$. The cell–cell adhesion term $f(\sigma_1, \sigma_2)$ depends on the clock values of the adjacent lattice sites with indices

Table 1 Parameter table. An asterisk * marks parameter values taken from *Zhang et al. (2011)*.

Parameter	Value	Description
Lattice dimensions	126×126	Cartesian (square) lattice size with periodic boundary conditions
T	20	Temperature*
θ_0	$U([0, 2\pi])$	Uniform initial distribution of initial clock phases
A_{target}	25	Target cell area*
λ	25	Area constraint coefficient*
ω	0.001	Clock speed
J_{MM}	0	Medium–medium contact local product adhesion energy*
$J_{CM} = J_0$	16	Medium-cell contact local product adhesion energy*
	2	Neighbor order*
N	445	Cell count

σ_1 and σ_2 and is given by

$$f(\sigma_1, \sigma_2) = \begin{cases} J_0(1 - J\cos(\theta_{\sigma_1} - \theta_{\sigma_2})) & \text{if } \sigma_1 \neq 0 \text{ and } \sigma_2 \neq 0 \\ J_0 & \text{if } \sigma_1 = 0 \text{ or } \sigma_2 = 0 \end{cases} \tag{2}$$

Recall that the index $\sigma = 0$ represents extracellular matrix, which has a contact energy of J_0. The parameter J encodes the effect of clock phases on adhesion. For $J > 0$, the function $f(\sigma_1, \sigma_2)$ is minimized when $\theta_{\sigma_1} = \theta_{\sigma_2}$, so cells of like clock phases adhere to each other the strongest ("like attracts like"). For $J < 0$ in contrast, $f(\sigma_1, \sigma_2)$ is minimized when $\theta_{\sigma_1} = \theta_{\sigma_2} + \pi$, and so then cells of opposite clock phases adhere to each other strongest ("opposites attract").

Time evolution is modeled *via* so-called spin flips. For this, a lattice site is selected randomly and it is proposed to change its index to that of a neighboring lattice site. Such a spin flip is accepted with a probability that depends on the change in the Hamiltonian function $\Delta\mathcal{H}$ it would entail. Specifically, it is given by

$$\text{Prob}(\text{spin flip}) = \begin{cases} 1 & \text{if} \quad \Delta\mathcal{H} \leq 0 \\ e^{-\Delta\mathcal{H}/T} & \text{if} \quad \Delta\mathcal{H} > 0 \end{cases} \tag{3}$$

where T is the so-called temperature of the system. Higher temperatures make it more likely for spin flips to occur but also make it more likely for cells to fragment, dissolving into each other. A Monte Carlo Step (MCS) consists of the number of spin flips corresponding to the total number of sites in the lattice. Simulation time is commonly measured in MCS.

Each cell $s = 1, \ldots, N$ in the model has an internal oscillating clock. For each cell $s = 1, \ldots, N$, we update its cell clock θ_s^t each MCS *via*

$$\theta_s^{t+1} = \theta_s^t + \omega \cdot (1 + K \cdot \frac{1}{\#\text{ neighbors of } s} \sum_{\text{neighbor } u \text{ of } s} \sin(\theta_u - \theta_s)) \tag{4}$$

Note that a cell's internal clock advances at the uniform clock speed ω, but is additionally influenced by the clocks of its neighbors in a Kuramoto-type way (*Kuramoto, 1984*). Here K is the clock coupling strength between neighboring cells. It controls how neighboring cells'

Table 2 Meaning of parameters J and K.

Parameter	Sign	Effect
J	$J > 0$	Adherence strongest for same clock phase ("Like attracts like")
	$J < 0$	Adherence strongest for opposite clock phases ("Opposites attract")
K	$K > 0$	"Neighbors seek to synchronize"
	$K < 0$	"Neighbors seek to anti-synchronize"

clocks influence each other. For $K > 0$, neighboring cells seek to synchronize their clock phases. For $K < 0$, neighboring cells seek to anti-synchronize their clocks.(The meanings of the crucial parameters J and K are summarized in Table 2.) As in other models (*OKeeffe, Hong & Strogatz, 2017*; *Glimm & Gruszka, 2024*), we note that all equations only depend on *differences* of clock phases, so that they are invariant under shifts in clock phase space in the form $\theta_s^t \to \theta_s^t - \omega \cdot t$. Effectively, this means we can assume that the uniform clock speed is zero and that only the terms with the $K-$factor in the update Eq. (4) enter into changes of the clocks at each MCS. In this sense, the choice of ω actually does not enter into the calculation apart from scaling K.

Parameters

The aim of our model is a high-level generic investigation of the interplay of adhesion and synchronization with minimal assumptions. Since it is not modeled on a concrete experimental setup, we chose to adopt the approach of *Zhang et al. (2011)*, who used CPM simulations to investigate and validate Steinberg's differential adhesion hypthesis (*Steinberg & Takeichi, 1994*). The parameter values *Zhang et al. (2011)* chose are based on experimental studies by *Armstrong (1971)* and *Steinberg & Takeichi (1994)*. Armstrong used retinal cells from chicken embryos, Steinberg used mouse L-cells. The paraments of *Zhang et al. (2011)* were not the result of direct measurements, but calibrated *via* matching quantities such as cell size and velocity distributions of individual cells to retinal cell data (*Mombach et al., 1995*; *Mombach & Glazier, 1996*) and ensuring that cells do not fragment. Our parameter values are indicated in Table 1. The lattice length scale is approximately 2 μm per pixel, the time scale is about 10,000 MCS per hour (*Zhang et al., 2011*). Note that our confluency is 70%, a typical value for *in vitro* experiments. Our oscillator velocity $\omega = 0.001$(clock change per MCS) corresponds to a period of about 7,000 MCS and thus very roughly on the order of one hour. This is the same order of magnitude as oscillations of Hes1 expression in somitogenesis (*Kageyama, Ohtsuka & Kobayashi, 2007*). We point out that in our model, only the *differences* between clock phases of neighboring cells matters for dynamical updates. Since all oscillators are assumed to have the same clock velocity ω, this means that simulations are actually independent of the value of ω and only depend on the effective value of the clock coordination parameter K. Accordingly, in our graphs, the color of the cells correponds to the phase *shift* relative to a clock that advances at a steady speed ω. We acknowledge that this independence of our simulation results on ω breaks

down if we drop the assumption that every cell has the exact same speed in favor of a more realistic distribution of speeds, but this is outside the scope of the current work.

Order parameters for characterizing phases

In the Results section, we will show that our model displays qualitative different types of behaviors for different choices of the parameters J and K. This is analogous to phase states in statistical physics. Phase transitions are often described quantitatively by order parameters, appropppriately defined quantities that characterize the state of the system; see *e.g.*, *Nolting (2018)*. We define here three order parameters for our model. In the Results section, we will use these to characterize the phases.

The first order parameter is a classical parameter quantifying synchronization due to *Kuramoto (1984)*. It is given by

$$r_{\text{global}} = \left| \frac{1}{N} \sum_{j=1}^{N} e^{i\theta_j} \right| \tag{5}$$

where N is the total number of cells in the simulation. The resulting r_{global} then satisfies $0 \leq r_{\text{global}} \leq 1$. The parameter r_{global} quantifies how synchronized all cells' clocks are at a specified MCS. If $r_{\text{global}} = 1$, all the cells' clocks are synchronized. If $r_{\text{global}} = 0$, all the cells' clocks are entirely unsychronized or anti-synchronized, meaning that all of their values are spread around the time clock evenly such that all values cancel each other out or there are synchronized groups of opposite phases that cancel each other out.

The second order parameter is a local version of r_{global}. For each cell, we compute a modified $r-$value *via* an average over its nearest neighbors (order 2). These values are then averaged over all cells:

$$r_{\text{local}} = \frac{1}{N} \sum_{\text{cell}\, k} \left| \frac{1}{s_k} \sum_{\text{neighbor } j \text{ of } k} e^{i\theta_j} \right| \tag{6}$$

where the first sum is taken over all cells in the simulation, s_k is the number of neighbors (order 2) of cell k and the second sum is taken over all neighbors of cell k. Note that $r_{\text{global}} = 1$ (complete global synchronization) implies $r_{\text{local}} = 1$, but not vice versa. Also note that complete randomness of phases does not typically lead to $r_{\text{local}} = 0$ because the second sum in the Eq. (6) is taken over a relatively small number, leading to large random variations. Numerically, we found that incoherence corresponds to a value of r_{local} of roughly 0.2; see also the discussion in the subsection "Phase Diagram".

The third order parameter ("checkerboard parameter") quantifies the extent to which neighboring cells' clock phases are in opposite phase (phase difference π). We need some tolerance since neighboring cells will not be completely in opposite phase all the time. We chose a tolerance of 6.25% from total anti-synchronization between neighboring cells. More explicitly,

$$\psi = \text{total number of pairs of neighboring lattice sites } (k,j)$$
$$\text{such that } \theta_k - \theta_j \in \left[\pi - \frac{\pi}{8}, \pi + \frac{\pi}{8}\right] \text{ (modulo } 2\pi\text{)}$$

Computational implementation

To implement the Cellular Potts Model, we used the open-source software CompuCell3D, version 4.2.5 (*Swat et al., 2012*) on a standard PCs (Intel(R) Core(TM) i5-6600 CPU @ 3.30 GHz, 16 GB RAM). Further analysis of the simulation data and generation of graphics were performed with Matlab. Figure 2 displays the results of 49 simulation runs, each of which took roughly 8–10 h individually.

RESULTS

Phase diagram

We concentrate on investigating the effects of the two parameters J and K encoding the interactions of clock synchronization and cell–cell adhesion. See Table 2 for the physical meaning of these parameters. The ranges $-1 < K < 1$ and $-1 < J < 1$ are meaningful for simulations[1]. Starting with random initial conditions for cell positions and clock values, we ran simulations to determine the long-term behavior for different values of J and K. The results are summarized in the phase diagram in Fig. 2. We used movies of the simulations to confirm that the simulation duration of 250,000 MCS was sufficiently long to guarantee convergence to an obvious phase state; see also Section "Dynamics of Synchronization". (Movies of all simulations are available online on the Zenodo repository at DOI 10.5281/zenodo.10681751).

The phase diagram in Fig. 2 clearly displays qualitatively different types of behaviors. To investigate these phases, we use the three order parameters defined in Order Section "Parameters for Characterizing Phases". Their heat maps are shown in Fig. 3. Note that all except r_{local} display very sharp step-like transitions between small and large values. This allows to quantify the different phases. We identify four different phases: The first is characterized by large r_{global}. We call it "global synchronization." Large values of the checkerboard parameter ψ characterize another phase, which we call "anti-synchronization." (Specifically, we can consider $\psi > 1000$.) There are two more phases, which we call "incoherence" and "local synchronization". The transition between incoherence and local synchronization is more gradual as clusters of synchronized cells become smaller with decreasing negative K. Nevertheless, we can utilize the parameter r_{local} to distinguish between definite local synchronization ($r_{\text{local}} \approx 1$) and definite incoherence ($r_{\text{local}} \approx 0.2$).

Figure 4 summarizes the phases. Global synchronization in the right half $K > 0$[2] and anti-synchronization (checkerboard pattern) in the quadrant $J < 0, K \leq 0$ are both readily visibly identifiable. This is straightforward to understand: For $K > 0$, neighboring cells seek to synchronize; and since all cells adhere to each other, this eventually leads to global synchronization for all values of J. (The dynamics of synchronization differ by whether J is positive or negative though; we investigate this in "Dynamics of Synchronization".) The anti-synchronized phase state is characterized by cells of opposite phases attracting each other ($J < 0$). Furthermore, cells seek to anti-synchronize with their neighbors (for $K < 0$). The resulting behavior is a checkerboard-style distribution of cell phases where cells minimize their energy by surrounding themselves with cells of the opposite phase.

[1] For $K \geq 1$ or $K \leq -1$, individual clocks can stop or run backwards; see Eq. (4). Values of J with $J > 1$ or $J < -1$ mean nonpositive cell–cell interaction energies. This means that lattice sites corresponding to the same cell can have higher interaction energies than sites corresponding to different cells. This causes fragmentation of cells, an unphysical behavior.

[2] Note that not all images in Fig. 2 for $K > 0$ show perfect global synchronization, but we verified that all approached synchronization eventually if simulations are allowed to continue; see also Fig. 6.

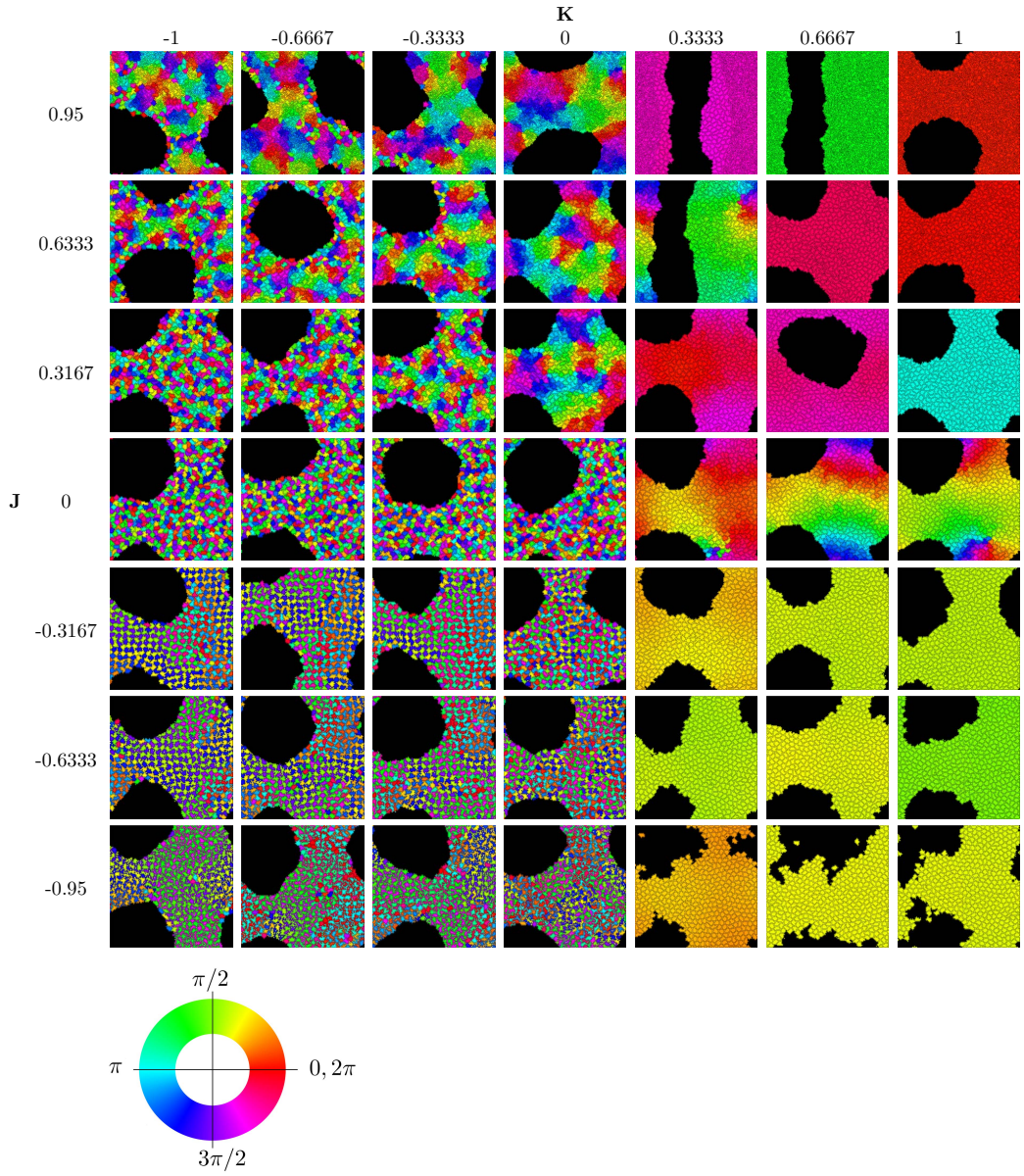

Figure 2 Parameter sweep of the model showing the state after 250,000 MCS. Cells are colored according to their clock phase. (Specifically, the colors show the clock phase difference relative to a standard clock moving at constant clock speed ω starting at 0.) Values shown are $J \in \{-0.95, -0.6333, -0.3167, 0, 0.3167, 0.6333, 0.95\}$ and $K \in \{-1, -0.6667, -0.3333, 0, 0.3333, 0.6667, 1\}$. Simulation runs were each of $N = 445$ cells and identical initial conditions (random distribution of clock phases).

Full-size DOI: 10.7717/peerj.16974/fig-2

The other two phases (local synchronization (synchronized spatial clusters) and incoherence (quasi-random spatial distribution of phases)) both occur in the quadrant $J \geq 0, K \leq 0$. For very negative K and small J, we have incoherence. In the case large J and K close to 0, cells tend to sort by phases and clusters de-synchronize sufficiently slowly that persistent locally synchronized clusters form.

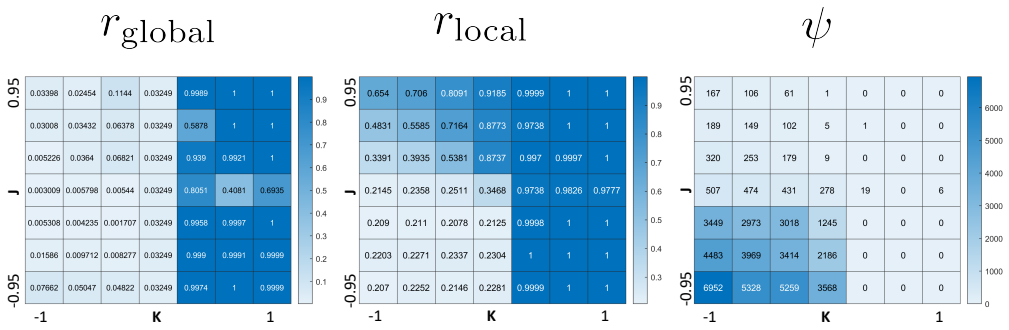

Figure 3 Heat maps of the three order parameters (r_{global}, r_{local}, checkerboard parameter ψ). Note the jump-like transitions along the lines $K = 0$ for r_{global}, as well as $J = 0$ and $K = 0$ for ψ. There is a similar sharp sharp transition of r_{local} along $K = 0$ for $J < 0$ and a curve in the quadrant $J > 0, K \leq 0$. This separates the parameter space into four phases: global synchronization ($r_{\text{global}} \approx 1$); local synchronization ($r_{\text{local}} \approx 1, r_{\text{global}} = 0$); antisynchronization (checkerboard pattern) (large ψ); and incoherence (all order parameters "small", see Fig. 4).

Full-size DOI: 10.7717/peerj.16974/fig-3

Movies show that global synchronization and anti-synchronization are essentially static distributions, where the cells' positions and shapes fluctuate, but the overall spatial distribution of clock phases stays the same. Incoherence and local synchronization are dynamic phases, where cells or cell clusters in different clock phases constantly move relative to each other, yielding a behavior in which each snapshot in time is different, but characteristic of the typical distribution.

To further characterize the incoherence phase, we compared the resulting distributions of clock values to the distribution obtained by chance. The results are summarized in Fig. 5. Note that the distributions of clock values for the incoherent phase is essentially indistinguishable to a uniform random distribution on the interval $[0, 2\pi)$. There is a marked difference to the anti-synchronization (checkerboard) phase, with two peaks at the distance π. Interestingly, the "local synchronization" case also gives a distribution indistinguishable from chance. This is because in the representation of Fig. 5, all spatial information is lost, so spatially completely mixed clock phases and spatially clustered clock phases give similar distributions.

Dynamics of synchronization

For positive values of K, cells' clocks eventually globally synchronize as shown in Fig. 2. When we investigated the dynamical paths to synchrony however, we found substantial qualitative differences depending on the sign of the parameter J (positive, negative or zero). Figure 6 illustrates this with $K = 1$ and three different values of J. To quantify the initial progress of synchronization for different values of J, Fig. 7A shows the order parameter r_{global} over time (MCS) up to 20,000 MCS. There is a clear hierarchy of J-values –the speed of synchronization is highest for the most negative value of J and decreases with increasing J with $J = +0.95$ corresponding to the slowest rate of progress. This can be seen also by the first two columns in Fig. 6. Why is this? Again, Fig. 6 provides an important insight: For negative J, "opposites attract" and hence at $t = 10,000$ MCS, it is clearly visible that

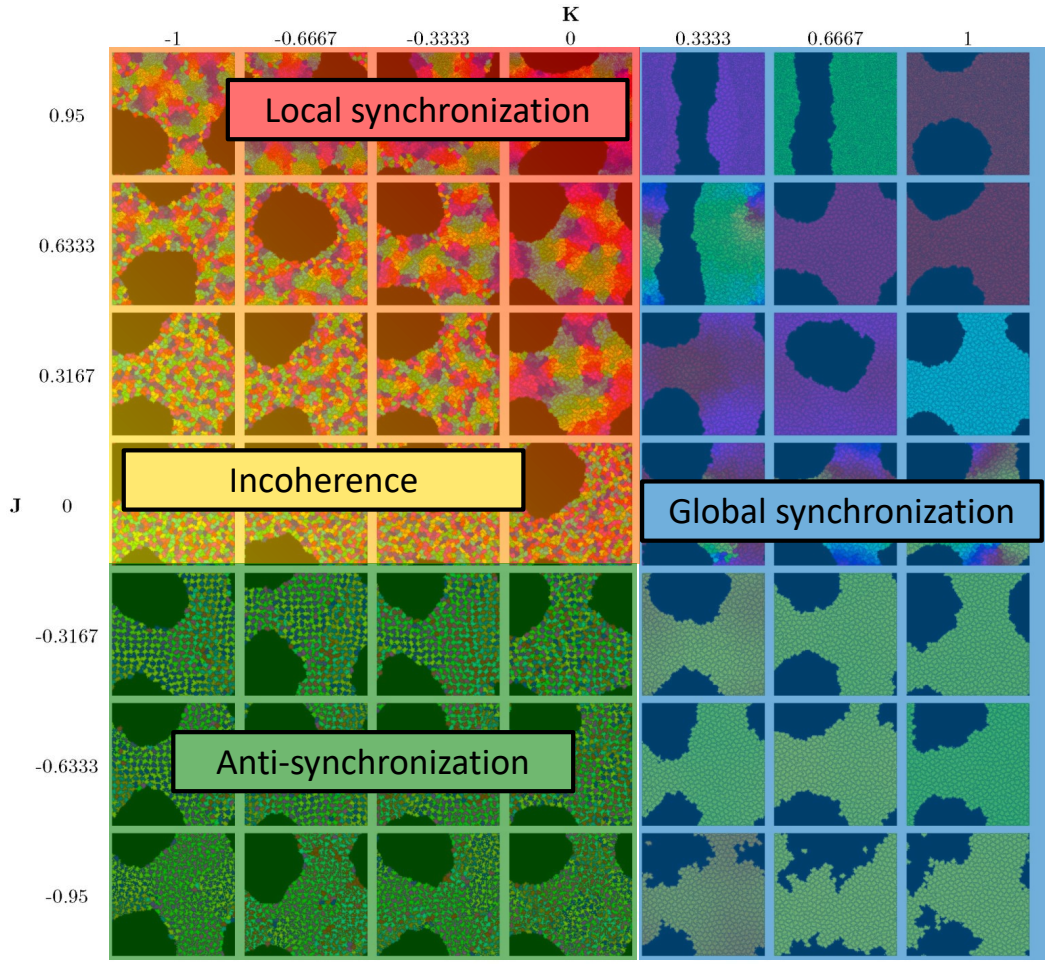

Figure 4 **Diagram of the four phases of the model.** See Fig. 3 for order parameters.
Full-size DOI: 10.7717/peerj.16974/fig-4

for $J = -0.95$, there are large regions of synchronized cells with cells of the opposite phase interspersed. (For example regions of orange cells with interspersed small blue cells, some slightly fragmented.) This proximity of cells of opposite clock phases early on leads to rapid synchronization. In contrast, this is not the case for $J = +0.6333$ (positive J, so "like attracts like") or $J = 0$ (clock phase has no influence on adhesion). One also observes that synchronized regions have more gradual transitions for $J = 0$ than for $J = +0.6333$. For instance for $J = +0.6333$, red and green cells tend to be separated by much smaller buffers of yellow and orange cells than is the case for $J = 0$.

These observations can be quantified *via* the local parameter r_{local}, shown in Fig. 7C: Here, the order is reversed and initially, the smaller J, the slower the rate of *local* synchronization. For negative J ("opposites attract"), the local synchronization even decays before increasing again.

The long-term rate of synchronization is plotted in Fig. 7B. The relationship between order of $J-$values and speed of synchronization seen in Fig. 7A is not preserved in the

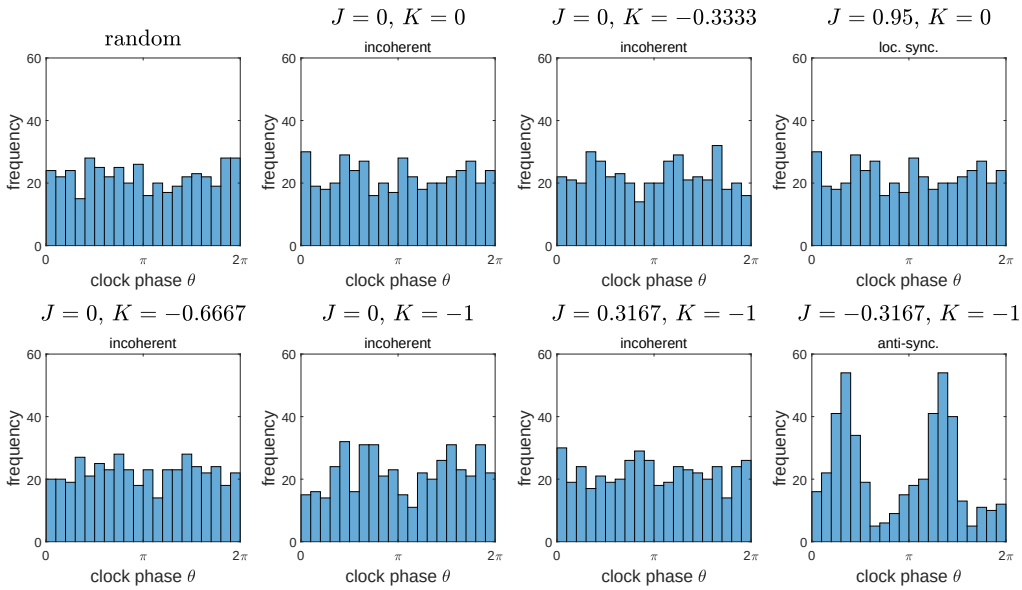

Figure 5 Histograms of distributions of clock phases for some of the simulations from Fig. 2. Each of the $N = 445$ cells gives one data point in the interval $[0, 2\pi)$. We used 20 bins. Here "random" denotes a random sample obtained by choosing $n = 445$ random numbers in $[0, 2\pi)$ with uniform probability distribution. Note that the resulting distributions for the "incoherent" phase data is essentially indistinguishable from the random distribution. Interestingly, the same is true for the example of the "locally synchronized" phase, but not the "anti-synchronized" (or checkerboard) phase, which is bimodal.

Full-size DOI: 10.7717/peerj.16974/fig-5

long run. Some of this may be due to the small sample size ($n = 10$). However, it is very clear that synchronization progresses most slowly for $J = 0$, the case where clock phase does not influence adhesion. At 250,000 MCS, complete synchronization had not been reached. (Illustrated also in Fig. 6 and Fig. 4.) This is in contrast to positive or negative values of J, where complete synchronization was achieved at that time. (Even for $J = 0$, synchronization was eventually achieved if the simulation was allowed to keep running; see time $t = 400,000$ MCS in Fig. 6.)

Why is synchronization especially slow for $J = 0$? An intuitive explanation is as follows: Synchronization proceeds especially fast (for positive K) if the clock phase distribution has sharp spatial gradients, *i.e.,* if many cells of very different clock phases are neighbors. In contrast, configurations with shallow clock gradients (gradual transitions of clock values) exhibit slower synchronization. With this principle, it is clear that for negative J, "opposites attract" and one indeed gets fields of cells with sharp clock gradients which synchronize quickly, as we noted before. But also the case of positive J ("like attracts like") creates sharp gradients, but with a different mechanism: Early on, synchronized clusters form as cells with similar phases effectively move towards each other. Because of cell–cell adhesion, these clusters have relatively sharply defined edges (Fig. 6), meaning sharp clock gradients, again leading to faster synchronization. In contrast, for $J = 0$, clock gradients are much more gradual, allowing regions of different clock phases to persist longer.

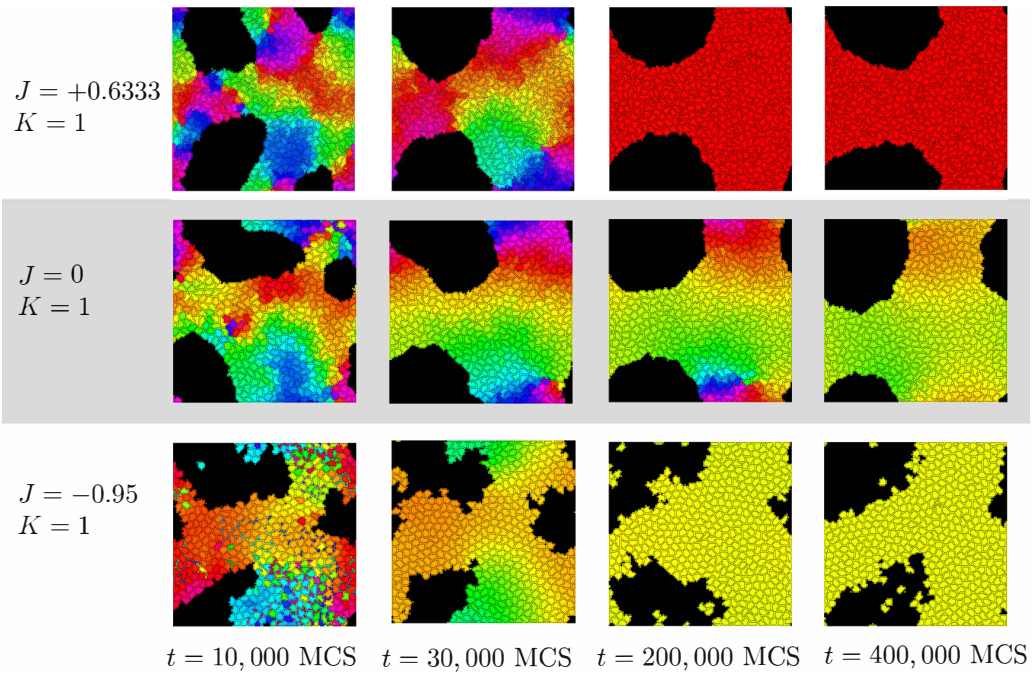

Figure 6 **Progress of synchronization for $K = 1$ and different values of J.** Cells are colored by the clock phase difference relative to a standard clock moving at constant clock speed ω as in Fig. 2.
Full-size DOI: 10.7717/peerj.16974/fig-6

DISCUSSION

We proposed a model of synchronization and aggregation of individual oscillators. In contrast to previous models (*OKeeffe, Hong & Strogatz, 2017*; *Glimm & Gruszka, 2024*), the oscillators were not just point particles, but entities with extended, fluctuating boundaries motivated by the behavior of biological cells *in vitro* (*Zhang et al., 2011*). We found four distinct phase states on which a simulation run can settle into depending on the parameters J and K values. By changing whether or not cells seek to synchronize or anti-synchronize with their neighbors (K) and whether or not cells seek out others with the same or opposite phase (J), we found cells globally synchronize, only locally synchronize, globally anti-synchronize, or remained incoherent. The anti-synchronization phase ("checkerboard pattern") is not found in the previous models with point particles and thus is made possible because of spatially extended cells.

For $K > 0$, we observed eventual global synchronization. The dynamics of synchronization differ by the parameter J though. Synchronization happens fastest for $J < 0$, the case where cells of opposite clock phases adhere most strongly. Indeed, there is a short transitory checkerboard pattern that quickly gives rise to uniform synchrony. This does not happen for $J \geq 0$. Most surprisingly though is the result that synchronization happens the slowest in the case of $J = 0$, when mixing of cells is purely diffusive. In this case, shallow gradients of clock phases appear which persist for much longer than the sharper gradients for $J > 0$ or $J < 0$.

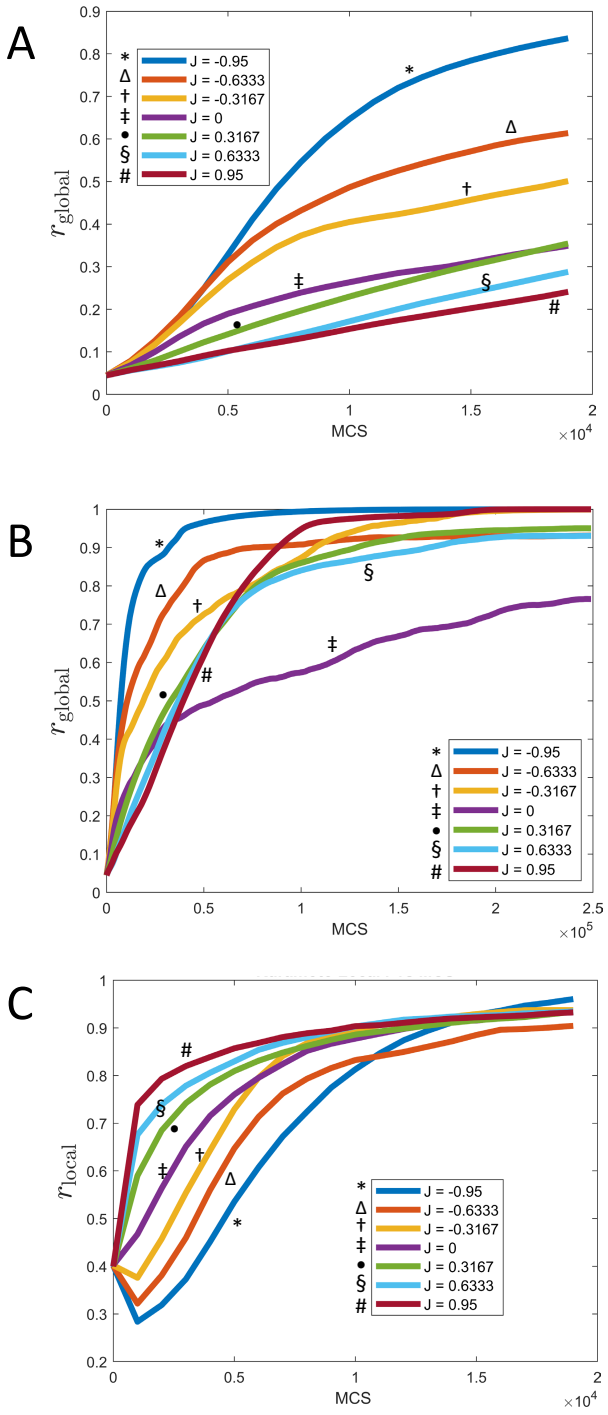

Figure 7 **Synchronization of cells over time for different values of J and fixed $K = 1$.** (A) Parameter r_{global} as a function of time (MCS) up to $t = 20,000$ MCS, covering the initial phase of synchronization. (B) Parameter r_{global} as a function of time (MCS) up to $t = 250,000$ MCS, covering the long term behavior. (C) Parameter r_{local} as a function of time (MCS) up to $t = 20,000$ MCS, covering the initial phase of synchronization. (All graphs are based on $n = 10$ runs for each curve.).

Full-size DOI: 10.7717/peerj.16974/fig-7

The possibility of persistent checkerboard patterns as one of the phases in our model is particularly interesting, since such checkerboard patterns are found *in vivo* in the auditory sensory epithelium of the cochlea of many species, composed of sensory hair cells and supporting cells (*Togashi et al., 2011*; *Katsunuma et al., 2022*). Both hair cells and supporting cells differentiate from pluripotent ectodermal cells (*Wan, Corfas & Stone, 2013*). The spatiotemporal determination of cell fate is arguably not completely understood, but it is influenced by members of the Hes/Hey genes, such as Hes1, which is known to undergo oscillatory expression in many developmental processes (*Tateya et al., 2011*; *Hirata et al., 2002*). Hes1 is thought to inhibit differentiation into hair cells. When Hes1 is knocked out, the checkerboard pattern is disturbed and in fact the number of hair cells is increased relative to the number of supporting cells (*Tateya et al., 2011*). Crucial for normal development is the expression of two adhesion molecules, nectin-1 and -3, which are produced by the hair cells and supporting cells. There is good evidence that heterotypic adhesion between these two cell types is the mechanism by which the checkerboard pattern is maintained. When nectin-3 was knocked out, the checkerboard pattern was disrupted, but there were still equal numbers of hair cells and supporting cells (*Togashi et al., 2011*).

Our model then gives a possible mechanism for the interplay of cell fate and spatial arrangements from an initially uniform field of pluripoptent cells, namely *via* intracellular oscillators such as Hes1 and their interplay with cell adhesion molecules. In this scenario, cells in a clock phase of high Hes1 expression would differentiate into supporting cells, those in a phase with low Hes1 expression into hair cells. Normal development then corresponds to the case of negative K (cells with high Hes1 suppress Hes1 production in neighboring cells) and negative J, meaning heterotypic adhesion. This yields a checkerboard pattern; see Fig. 2. The experiment of knocking out nectins by *Togashi et al. (2011)* then correspod to changing J from negative values to $J = 0$. This results in breaking up the checkerboard pattern into incoherent patterns, *i.e.,* patterns without a correlation between clock phase and spatial position. Note that in these patterns, clock phases are spatially mixed and there is no bias towards any clock phase (Fig. 5), which is consistent with the observation that the numbers of hair cells and supporting cells remained equal (*Togashi et al., 2011*).

These observations point to the possibility of interesting insights our simple model, or more elaborate variants of it, can provide. Still, we need to stress that the model is minimalistic in that we concentrate on two core interactions –synchronization and aggregation. The cost of this generality is specificity. For further work, tayloring the core model to specific phenomea such as pattern formation in the auditory sensory epithelium as sketched above requires refining and enhancing it by matching parameters, but also potentially including phenomena that are not part of our current generic model such as cell polarity, chemotaxis, or dealing explicitly with cell differentiation.

ADDITIONAL INFORMATION AND DECLARATIONS

Funding

Tilmann Glimm was supported by the John Templeton Foundation (#62220). The opinions expressed in this paper are those of the authors and not those of the John Templeton

Foundation. Rose Una was supported by a Jarvis Memorial Summer Research Stipend from Western Washington University. The funders had no role in study design, data collection and analysis, decision to publish, or preparation of the manuscript.

Grant Disclosures

The following grant information was disclosed by the authors:
The John Templeton Foundation: #62220.
A Jarvis Memorial Summer Research Stipend from Western Washington University.

Competing Interests

The authors declare there are no competing interests.

Author Contributions

- Rose Una conceived and designed the experiments, performed the experiments, analyzed the data, prepared figures and/or tables, authored or reviewed drafts of the article, code development and implementation, and approved the final draft.
- Tilmann Glimm conceived and designed the experiments, performed the experiments, analyzed the data, prepared figures and/or tables, authored or reviewed drafts of the article, code development and implementation, and approved the final draft.

Data Availability

The following information was supplied regarding data availability:

The CompuCell3d code for two specific parameter values for K and J is available in the Supplemental File. The code used for other values was equivalent.

Supplemental Information

Supplemental information for this article can be found online at http://dx.doi.org/10.7717/peerj.16974#supplemental-information.

REFERENCES

Alber MS, Jiang Y, Kiskowski MA. 2004. Lattice gas cellular automation model for rippling and aggregation in myxobacteria. *Physica D: Nonlinear Phenomena* **191(3)**:343–358 DOI 10.1016/j.physd.2003.11.012.

Arias Del Angel JA, Nanjundiah V, Benítez M, Newman SA. 2020. Interplay of mesoscale physics and agent-like behaviors in the parallel evolution of aggregative multicellularity. *EvoDevo* **11(1)**:1–18 DOI 10.1186/s13227-020-0147-0.

Armstrong PB. 1971. Light and electron microscope studies of cell sorting in combinations of chick embryo neural retina and retinal pigment epithelium. *Wilhelm Roux' Archiv für Entwicklungsmechanik Der Organismen* **168(2)**:125–141 DOI 10.1007/BF00581804.

Barciś A, Bettstetter C. 2020. Sandsbots: robots that sync and swarm. *IEEE Access* **8**:218752–218764 DOI 10.1109/ACCESS.2020.3041393.

Bhat R, Glimm T, Linde-Medina M, Cui C, Newman SA. 2019. Synchronization of Hes1 oscillations coordinates and refines condensation formation and patterning of the avian limb skeleton. *Mechanisms of Development* **156**:41–54 DOI 10.1016/j.mod.2019.03.001.

Boccaletti S, Pisarchik AN, Genio CID, Amann A. 2018. *Synchronization: from coupled systems to complex networks*. Cambridge: Cambridge University Press.

Bonner JT. 2008. The social amoebae. In: *The social amoebae*. Princeton, NJ: Princeton University Press.

Carraco G, Martins-Jesus AP, Andrade RP. 2022. The vertebrate Embryo Clock: common players dancing to a different beat. *Frontiers in Cell and Developmental Biology* **10**:944016 DOI 10.3389/fcell.2022.944016.

Cooke J, Zeeman EC. 1976. A clock and wavefront model for control of the number of repeated structures during animal morphogenesis. *Journal of Theoretical Biology* **58(2)**:455–476 DOI 10.1016/S0022-5193(76)80131-2.

Deneke VE, Melbinger A, Vergassola M, Di Talia S. 2016. Waves of Cdk1 activity in S phase synchronize the cell cycle in Drosophila embryos. *Developmental Cell* **38(4)**:399–412 DOI 10.1016/j.devcel.2016.07.023.

Dörfler F, Bullo F. 2014. Synchronization in complex networks of phase oscillators: a survey. *Automatica* **50(6)**:1539–1564 DOI 10.1016/j.automatica.2014.04.012.

Faust LF. 2010. Natural history and flash repertoire of the synchronous firefly Photinus carolinus (Coleoptera: Lampyridae) in the Great Smoky Mountains National Park. *Florida Entomologist* **93(2)**:208–217 DOI 10.1653/024.093.0210.

Frisch B, Koeniger N. 1994. Social synchronization of the activity rhythms of honeybees within a colony. *Behavioral Ecology and Sociobiology* **35(2)**:91–98 DOI 10.1007/BF00171498.

Glimm T, Gruszka D. 2024. Modeling the interplay of oscillatory synchronization and aggregation via cell-cell adhesion. *Nonlinearity* **37**:035016 DOI 10.1088/1361-6544/ad237a.

Graner N, Glazier N. 1992. Simulation of biological cell sorting using a two-dimensional extended Potts model. *Physical Review Letters* **69(13)**:2013–2016 DOI 10.1103/PhysRevLett.69.2013.

Gregor T, Fujimoto K, Masaki N, Sawai S. 2010. The onset of collective behavior in social amoebae. *Science* **328(5981)**:1021–1025 DOI 10.1126/science.1183415.

Guzzo M, Murray SM, Martineau E, Lhospice S, Baronian G, My L, Zhang Y, Espinosa L, Vincentelli R, Bratton BP, Shaevitz JW, Molle V, Howard M, Mignot T. 2018. A gated relaxation oscillator mediated by FrzX controls morphogenetic movements in *Myxococcus xanthus*. *Nature Microbiology* **3(8)**:948–959 DOI 10.1038/s41564-018-0203-x.

Hansel D, Mato G, Meunier C. 1995. Synchrony in excitatory neural networks. *Neural Computation* **7(2)**:307–337 DOI 10.1162/neco.1995.7.2.307.

Hirata H, Yoshiura S, Ohtsuka T, Bessho Y, Harada T, Yoshikawa K, Kageyama R. 2002. Oscillatory expression of the bHLH factor Hes1 regulated by a negative feedback loop. *Science* **298(5594)**:840–843 DOI 10.1126/science.1074560.

Jiang Y-J, Aerne BL, Smithers L, Haddon C, Ish-Horowicz D, Lewis J. 2000. Notch signalling and the synchronization of the somite segmentation clock. *Nature* **408**(**6811**):475–479 DOI 10.1038/35044091.

Kageyama R, Ohtsuka T, Kobayashi T. 2007. The Hes gene family: repressors and oscillators that orchestrate embryogenesis. *Development* **134**(**7**):1243–1251 DOI 10.1242/dev.000786.

Kageyama R, Shimojo H, Isomura A. 2018. Oscillatory control of notch signaling in development. *Advances in Experimental Medicine and Biology* **1066**:265–277 DOI 10.1007/978-3-319-89512-3_13.

Katsunuma S, Togashi H, Kuno S, Fujita T, Nibu K-I. 2022. Hearing loss in mice with disruption of auditory epithelial patterning in the cochlea. *Frontiers in Cell and Developmental Biology* **10**:1073830 DOI 10.3389/fcell.2022.1073830.

Kuramoto Y. 1984. *Chemical oscillations, waves and turbulence.* Berlin, Heidelberg: Springer-Verlag.

Marée AF, Hogeweg P. 2001. How amoeboids self-organize into a fruiting body: multicellular coordination in Dictyostelium discoideum. *Proceedings of the National Academy of Sciences of the United States of America* **98**(**7**):3879–3883.

Mombach JC, Glazier JA, Raphael RC, Zajac M. 1995. Quantitative comparison between differential adhesion models and cell sorting in the presence and absence of fluctuations. *Physical Review Letters* **75**(**11**):2244–2247 DOI 10.1103/PhysRevLett.75.2244.

Mombach JCM, Glazier JA. 1996. Single cell motion in aggregates of embryonic cells. *Physical Review Letters* **76**(**16**):3032–3035 DOI 10.1103/PhysRevLett.76.3032.

Murata A, Hayashi S-I. 2016. Notch-mediated cell adhesion. *Biology* **5**(**1**):5 DOI 10.3390/biology5010005.

Murray PJ, Maini PK, Baker RE. 2011. The clock and wavefront model revisited. *Journal of Theoretical Biology* **283**(**1**):227–238 DOI 10.1016/j.jtbi.2011.05.004.

Newman SA, Bhat R, Glimm T. 2021. Spatial waves and temporal oscillations in vertebrate limb development. *Biosystems* **208**:104502 DOI 10.1016/j.biosystems.2021.104502.

Nolting W. 2018. Classical statistical physics. In: Nolting W, ed. *Theoretical physics 8: statistical physics*. Cham: Springer International Publishing, 1–93 DOI 10.1007/978-3-319-73827-7_1.

O'Keeffe K, Ceron S, Petersen K. 2022. Collective behavior of swarmalators on a ring. *Physical Review E* **105**(**1**):014211 DOI 10.1103/PhysRevE.105.014211.

O'Keeffe KP, Hong H, Strogatz SH. 2017. Oscillators that sync and swarm. *Nature Communications* **8**(**1**):1504 DOI 10.1038/s41467-017-01190-3.

Peruani F, Starruß J, Jakovljevic V, Søgaard-Andersen L, Deutsch A, Bär M. 2012. Collective motion and nonequilibrium cluster formation in colonies of gliding bacteria. *Physical Review Letters* **108**(**9**):098102 DOI 10.1103/PhysRevLett.108.098102.

Pikovsky A, Rosenblum M, Kurths J. 2003. *Synchronization: a universal concept in nonlinear sciences*. 1st edition. Cambridge: Cambridge University Press.

Ramírez-Ávila GM, Kurths J, Depickère S, Deneubourg J-L. 2019. Modeling fireflies synchronization. In: Macau EEN, ed. *A mathematical modeling approach from*

nonlinear dynamics to complex systems. *Nonlinear systems and complexity*. Cham: Springer International Publishing, 131–156 DOI 10.1007/978-3-319-78512-7_8.

Rodrigues FA, Peron TKD, Ji P, Kurths J. 2016. The Kuramoto model in complex networks. *Physics Reports* **610**:1–98 DOI 10.1016/j.physrep.2015.10.008.

Sar GK, Chowdhury SN, Perc M, Ghosh D. 2022. Swarmalators under competitive time-varying phase interactions. *New Journal of Physics* **24(4)**:043004 DOI 10.1088/1367-2630/ac5da2.

Shimkets LJ, Kaiser D. 1982. Induction of coordinated movement of Myxococcus xanthus cells. *Journal of Bacteriology* **152(1)**:451–461 DOI 10.1128/jb.152.1.451-461.1982.

Siehler O, Wang S, Bloch G. 2021. Social synchronization of circadian rhythms with a focus on honeybees. *Philosophical Transactions of the Royal Society B: Biological Sciences* **376(1835)**:20200342 DOI 10.1098/rstb.2020.0342.

Singer W. 1999. Neuronal synchrony: a versatile code for the definition of relations? *Neuron* **24(1)**:49–65 111–125 DOI 10.1016/s0896-6273(00)80821-1.

Sokol J. 2022. How do fireflies flash in sync? Studies suggest a new answer. Quanta Magazine. *Available at https://www.quantamagazine.org/how-do-fireflies-flash-in-sync-studies-suggest-a-new-answer-20220920*.

Steinberg MS, Takeichi M. 1994. Experimental specification of cell sorting, tissue spreading, and specific spatial patterning by quantitative differences in cadherin expression. *Proceedings of the National Academy of Sciences of the United States of America* **91(1)**:206–209 DOI 10.1073/pnas.91.1.206.

Swat MH, Thomas GL, Belmonte JM, Shirinifard A, Hmeljak D, Glazier JA. 2012. Chapter 13—multi-scale modeling of tissues using CompuCell3D. In: Asthagiri AR, Arkin AP, eds. *Computational methods in cell biology*. *Methods in cell biology*, 110. Cambridge: Academic Press, 325–366 DOI 10.1016/B978-0-12-388403-9.00013-8.

Tateya T, Imayoshi I, Tateya I, Ito J, Kageyama R. 2011. Cooperative functions of Hes/Hey genes in auditory hair cell and supporting cell development. *Developmental Biology* **352(2)**:329–340 DOI 10.1016/j.ydbio.2011.01.038.

Thutupalli S, Sun M, Bunyak F, Palaniappan K, Shaevitz JW. 2015. Directional reversals enable Myxococcus xanthus cells to produce collective one-dimensional streams during fruiting-body formation. *Journal of the Royal Society Interface* **12(109)**:20150049 DOI 10.1098/rsif.2015.0049.

Togashi H, Kominami K, Waseda M, Komura H, Miyoshi J, Takeichi M, Takai Y. 2011. Nectins establish a checkerboard-like cellular pattern in the auditory epithelium. *Science* **333(6046)**:1144–1147 DOI 10.1126/science.1208467.

Uhlhaas P, Pipa G, Lima B, Melloni L, Neuenschwander S, Nikolić D, Singer W. 2009. Neural synchrony in cortical networks: history, concept and current status. *Frontiers in Integrative Neuroscience* **3**:17 DOI 10.3389/neuro.07.017.2009.

Una R. 2023. Biological oscillator synchronization with the Cellular Potts Model. Honors thesis, Western Washington University, Bellingham, WA.

Van Oss C, Panfilov AV, Hogeweg P, Siegert F, Weijer CJ. 1996. Spatial pattern formation during aggregation of the slime mould dictyostelium discoideum. *Journal of Theoretical BBology* **181(3)**:203–213 DOI 10.1006/jtbi.1996.0126.

Venzin OF, Oates AC. 2020. What are you synching about? Emerging complexity of Notch signaling in the segmentation clock. *Developmental Biology* **460(1)**:40–54 DOI 10.1016/j.ydbio.2019.06.024.

Wan G, Corfas G, Stone JS. 2013. Inner ear supporting cells: rethinking the silent majority. *Seminars in Cell & Developmental Biology* **24(5)**:448–459 DOI 10.1016/j.semcdb.2013.03.009.

Winfree AT. 1987. *The timing of biological clocks*. Vol. 19. New York, NY: Henry Holt and Co.

Zhang Y, Thomas GL, Swat M, Shirinifard A, Glazier JA. 2011. Computer simulations of cell sorting due to differential adhesion. *PLOS ONE* **6(10)**:e24999 DOI 10.1371/journal.pone.0024999.

Zusman DR, Scott AE, Yang Z, Kirby JR. 2007. Chemosensory pathways, motility and development in Myxococcus xanthus. *Nature Reviews Microbiology* **5(11)**:862–872 DOI 10.1038/nrmicro1770.